Open Archive TOULOUSE Archive Ouverte (OATAO)

Mass or heat transfer inside a spherical gas bubble at low to moderate Reynolds number

D. Colombet [a,b,c,d,e,f], D. Legendre [d,e,*], A. Cockx [a,b,c], P. Guiraud [a,b,c]

[a] Université de Toulouse, INSA, UPS, INP, LISBP, 135 Avenue de Rangueil, F-31077 Toulouse, France
[b] INRA, UMRA792 Ingénierie des Systémes Biologiques et des Procédés, F-31400 Toulouse, France
[c] CNRS, UMR5504, F-31400 Toulouse, France
[d] Université de Toulouse, INPT, UPS, IMFT (Institut de Mécanique des Fluides de Toulouse), Allée Camille Soula, F-31400 Toulouse, France
[e] CNRS, IMFT, F-31400 Toulouse, France
[f] Rhodia – Solvay, 85, Avenue des Fréres Perret, BP 62, 69192 Saint Fons, France

ABSTRACT

Mass (or heat) transfer inside a spherical gas bubble rising through a stationary liquid is investigated by direct numerical simulation. Simulations were carried out for bubble Reynolds number ranging from 0.1 to 100 and for Péclet numbers ranging from 1 to 2000. The study focuses on the effect of the bubble Reynolds number on both the interfacial transfer and the saturation time of the concentration inside the bubble. We show that the maximum velocity U_{max} at the bubble interface is the pertinent velocity to describe both internal and external transfers. The corresponding Sherwood (or Nusselt) numbers and the saturation time can be described by a sigmoid function depending on the Péclet number $Pe_{max} = U_{max}d_b/D$ (d_b and D being the bubble diameter and the corresponding diffusion coefficient).

1. Introduction

In a great number of processes such as chemical engineering or water treatment, bubbly flows are used for mass transfer. In some situations the resistance of the transfer resides in the gas phase. For physical absorption or desorption of very soluble gases, as predicted by the Lewis–Whitman two-film model [1], the mass transfer liquid-phase resistance can be negligible and mass transfer is then controlled by the gas phase resistance. A typical example is ammonia removal from water where mass transfer is limited by the solute concentration transport inside bubbles. For gas absorption followed by an extremely fast chemical reaction in the liquid phase, mass transfer can also be controlled by gas-side transfer resistance [2,3]. A typical example is sulfur dioxide absorption into alkali solutions. In such cases, the estimation of the mass transfer requires the knowledge of the gas-side transfer. A large amount of studies have considered the external mass transfer [4–7] but less attention has been paid to the internal mass transfer.

Newman [8] has derived the analytical solution of the mass transfer controlled by pure diffusion inside a sphere. From the instantaneous concentration profile, the time evolution of the in-side Sherwood number Sh has been obtained for a fixed concentration c_s at the surface and an initial uniform concentration c_0 inside the sphere. The corresponding Sherwood number tends to an asymptotic constant value $Sh_\infty = Sh(t \to \infty)$:

$$Sh_\infty(Re = 0, Pe = 0) = \frac{2\pi^2}{3} \approx 6.58 \qquad (1)$$

This solution can be used for a bubble fixed relative to the surrounding liquid i.e. for a bubble Reynolds number $Re = \rho_L U_b d_b / \mu_L = 0$ and a Péclet number $Pe = U_b d_b / D = 0$ where d_b is the bubble diameter, U_b is the bubble relative velocity, ρ_L is the liquid density, μ_L its dynamic viscosity and D is the diffusion coefficient. In practice, this solution is expected to be valid in the limits $Re \to 0$ and $Pe \to 0$.

Using the Stokes (or creeping flow) solution for the description of the flow inside the bubble [9,10], Kronig and Brink [11] obtained numerically the instantaneous Sherwood number in the limit of high Péclet number. The corresponding asymptotic value of the Sherwood number Sh_∞, valid in the limits $Re \to 0$ and $Pe \to \infty$, is also found to be constant:

$$Sh_\infty(Re \to 0, Pe \to \infty) \approx 17.90 \qquad (2)$$

As pointed out by Clift et al. [4], the solution (2) is very close to the solution (1) when considering an effective diffusion coefficient $D_{eff} = 2.5D$. The experiments of Calderbank and Korchinski [12] on

* Corresponding author at: Université de Toulouse, INPT, UPS, IMFT (Institut de Mécanique des Fluides de Toulouse), Allée Camille Soula, F-31400 Toulouse, France.
E-mail address: legendre@imft.fr (D. Legendre).

List of symbols

c	mass concentration, kg m^{-3}
c_s	saturation mass concentration, kg m^{-3}
c_0	initial mass concentration, kg m^{-3}
c'	dimensionless mass concentration, $c' = (c - c_0)/(c_s - c_0)$
$\langle c \rangle$	volume average concentration in the gas bubble, kg m^{-3}
C_D	bubble drag coefficient
d_b	bubble diameter, m
D	molecular diffusion coefficient, m^2 s^{-1}
F	dimensionless mass concentration, $F = \langle c \rangle/(c_s - c_0)$
J	surface average mass flux, kg m^{-2} s^{-1}
J_{loc}	local mass flux, kg m^{-2} s^{-1}
n	unit vector normal to the surface under consideration
p	pressure, Pa
Pe	Péclet number, $Pe = U_b d_b/D$
Pe_{eff}	effective Péclet number
Pe_{max}	Péclet number based on U_{max}, $Pe_{max} = U_{max}d_b/D$
r	radial coordinate
r'	dimensionless radial coordinate, $r' = r/r_b$
r_b	bubble radius $r_b = d_b/2$, m
R_∞	computational domain radius, m
Re	bubble Reynolds number, $Re = \rho_L U_b d_b/\mu_L$
Sc	Schmidt number, $Sc = v_G/D$
Sh	instantaneous Sherwood number
Sh_∞	asymptotic Sherwood number, $Sh_\infty = Sh(t \to \infty)$
Sh_∞^*	normalized asymptotic Sherwood number
t	time, s
t'	dimensionless time (Fourier number), $t' = tD/r_b^2$
t	unit vector tangential to the bubble surface

t_{sat}	saturation time, s
t'_{sat}	dimensionless saturation time, $t'_{sat} = t_{sat}D/r_b^2$
t_{sat}^*	normalized saturation time
u_k	velocity of phase k, m s^{-1}
U_{max}	maximal velocity at the bubble interface, m s^{-1}
U_b	bubble rising velocity, m s^{-1}
u_θ	local liquid velocity at the bubble surface, m s^{-1}

Greek symbols

δ_D	concentration boundary layer thickness, m
Δ_{in}	internal grid size at the interface, m
Δ_{out}	external grid size at the interface, m
μ_k	dynamic viscosity of phase k, Pas
μ^*	dynamic viscosity ratio, $\mu^* = \mu_G/\mu_L$
v_k	kinematic viscosity of phase k, m^2 s^{-1}
ρ_k	density of phase k, kg m^{-3}
ρ^*	density ratio, $\rho^* = \rho_G/\rho_L$
τ	viscous shear stress, Pa

Superscripts

ext	external transfer

Subscripts

G	gas phase
k	phase k
L	liquid phase

heat transfer inside bromobenzene circulating drops falling in water–glycerol solutions also show an agreement with relation (2) with a measured effective diffusion coefficient $D_{eff} = 2.25D$. Using the Hadamard–Rybczynski solution for the internal flow and numerical simulations for the transport of the mass concentration, Clift et al. [4] have shown that the increase of the Péclet number produces a gradual increase of the asymptotic Sherwood number Sh_∞, from the value $Sh_\infty \approx 6.58$ given by (1) up to a value close to $Sh_\infty \approx 17.90$ given by (2).

Few studies have considered the internal transfer at moderate Reynolds number [13,14]. The numerical simulations performed by Oliver and De Witt [13] indicate that the Sherwood number Sh_∞ at large Péclet number weakly increases with the bubble Reynolds number Re. For intermediate Reynolds number, Sh_∞ is influenced by both the Péclet and the Reynolds numbers. In order to describe the corresponding evolution of Sh_∞, Oliver and De Witt [13] introduced the following effective Péclet number Pe_{eff} expressed here for a spherical bubble:

$$Pe_{eff} = [1 + 0.4 \log(0.3\,Re + 1)]\,Pe \qquad (3)$$

This effective Péclet number expresses the increase of the inner vortex strength with the bubble Reynolds number. Considering this effective Péclet number, Oliver and De Witt [13] show that their numerical results almost collapse on a single curve. Note that the increase of the asymptotic Sherwood number Sh_∞ with the Reynolds number has also been reported by Paschedag et al. [15] for the conjugate mass transfer problem inside droplets.

More recently, thanks to direct numerical simulations, Juncu [14] investigated thoroughly unsteady heat/mass transfer inside a circulating sphere for three fluid–fluid systems (gas-bubbles, liquid drops in an immiscible liquids, liquid drops in gases). For the case of a bubble, this work has considered $Re \leqslant 100$ and

$Pe \leqslant 10^4$. The simulations confirm the increase of the Sherwood number with the increase of the bubble Reynolds number. The study also shows that the scaling proposed by Oliver and De Witt [13] (Eq. (3)) is only adapted for the description of the transfer for small to moderate effective Péclet number, i.e. $Pe_{eff} \leqslant 200$.

In order to determine the transfer in the limit of high Reynolds numbers, Zaritzky and Calvelo [16] have used the internal potential flow solution [17] for the flow inside the bubble in order to solve by numerical simulation the concentration field. Surprisingly, Sh_∞ is close to the value 17.90 given by (2) in the limit of small Reynolds number [11] suggesting no effect of the Reynolds number on the transfer at high Péclet number. Despite a good agreement found between these numerical results and their experimental measurements for the transfer of SO$_2$ in water for $Re > 800$, this results is in contradiction with the numerical simulations [13,14] indicating an effect of the Reynolds number on the inside transfer. According to Oliver and De Witt [13], this effect is linked to the non uniform increase of the velocity around a fluid sphere when increasing the Reynolds number. The main objective of this paper is to clarify the effect of the bubble Reynolds number on the transfer at intermediate Reynolds number. For this purpose direct numerical simulations have been performed to calculate the inside transfer for bubble Reynolds numbers ranging from 0.1 to 100 and for Péclet numbers ranging from 1 to 2000.

The paper is organized as follows. Sections 2 and 3 present the governing equations and the numerical procedure, respectively. Section 4 is devoted to the validation of the numerical procedure for both the fluid motion and the internal transfer. Section 5 presents and discusses the numerical results in order to improve the modeling of the internal transfer. The modeling of the Sherwood number for external mass (or heat) transfer is also discussed.

2. Governing equations

We consider a clean spherical gas bubble of diameter $d_b = 2r_b$ moving at a constant relative velocity U_b in a liquid at rest. In terms of a (Eulerian) frame of reference fixed with the bubble, the liquid velocity field inside ($k = G$) and outside ($k = L$) the bubble is given by the Navier–Stokes equations written for Newtonian incompressible fluids:

$$\nabla \cdot u_k = 0 \tag{4}$$

$$\rho_k \left(\frac{\partial u_k}{\partial t} + u_k \cdot \nabla u_k \right) = -\nabla p_k + \nabla \cdot \tau_k \tag{5}$$

where $\tau_k = \mu_k (\nabla u_k + \nabla^T u_k)$ is the viscous part of the stress tensor, ρ_k and μ_k are the density and the dynamic viscosity of the fluid k, respectively.

Far from the bubble, the external liquid satisfies the condition $u_L \to -U_b$. In the absence of any surface tension gradient and bubble deformation, the two fluids satisfy the continuity of the normal velocity, the tangential velocity and the tangential viscous stress at the bubble surface:

$$u_L \cdot \mathbf{n} = u_G \cdot \mathbf{n} = 0$$
$$u_L \cdot \mathbf{t} = u_G \cdot \mathbf{t} \tag{6}$$
$$\mathbf{n} \times \tau_L \cdot \mathbf{n} = \mathbf{n} \times \tau_G \cdot \mathbf{n}$$

where $\mathbf{n}$ and $\mathbf{t}$ are unity vectors normal and tangent to the bubble surface.

The advection–diffusion equation for the concentration c inside the bubble is

$$\frac{\partial c}{\partial t} + \nabla \cdot (c\, u_G) = D\nabla^2 c \tag{7}$$

where D is the diffusion coefficient of the considered species in the gas filling the bubble. The initial concentration inside the bubble is noted c_0 and c_s is the concentration set fixed at the bubble surface. Some results will be presented using the normalized concentration $c' = (c - c_0)/(c_s - c_0)$ as a function of the Fourier number $t' = Dt/r_b^2$ and the normalized radial position $r' = r/r_b$. The transfer inside the bubble is characterized using the instantaneous surface average Sherwood number:

$$Sh(t) = \frac{J d_b}{D(c_s - \langle c \rangle)} \quad \text{with } J = \frac{1}{\pi d_b^2} \oint J_{loc}\, ds, \tag{8}$$

where J is the surface average mass flux, $J_{loc} = -D(\partial c/\partial n)$ is the local mass flux at the interface and $\langle c \rangle$ is the instantaneous volume average concentration inside the bubble. The average Sherwood number defined by (8) is directly linked to the volume average dimensionless concentration $F = \langle c \rangle/(c_s - c_0)$ by the relation [4]:

$$Sh(t') = \frac{2}{3(1 - F)} \frac{dF}{dt'} \tag{9}$$

In this work, the instantaneous Sherwood number has been calculated using this relation. We also introduce the asymptotic Sherwood Sh_∞ number as $Sh_\infty = Sh(t \to \infty)$. Note that the instantaneous Sherwood number always reaches the asymptotic value Sh_∞ for a time t' smaller than 0.5 for all the values (Re, Pe) considered in this work.

The transfer is studied as a function of the bubble Reynolds number Re

$$Re = \frac{\rho_L U_b d_b}{\mu_L} \tag{10}$$

and the Péclet number Pe

$$Pe = \frac{U_b d_b}{D} \tag{11}$$

This Péclet number compares the characteristic time of diffusion d_b^2/D to the characteristic time of advection at the interface d_b/U_b. We also introduce the Schmidt number $Sc = v_G/D$ where $v_G = \mu_G/\rho_G$ is the gas kinematic viscosity. The simulations reported in this study were performed for the density and viscosity ratio $\rho^* = \rho_G/\rho_L = 0.0012$ and $\mu^* = \mu_G/\mu_L = 0.018$, respectively.

3. Numerical procedure

The flow generated by a clean spherical bubble moving at a constant velocity in a liquid at rest is steady and axisymmetric whatever the bubble Reynolds number [18]. As a consequence, the system of Eq. (4)–(7) has been solved in an axisymmetric system of coordinates. The equations have been written in dimensionless primitive variables and solved with *Comsol*® 3.5a using the Galerkin type finite element method with a direct linear solver [19]. Finite elements used in this work are second-order Lagrange elements. The time integration is implicit using variable-order backward differentiation formulas up to filth order according to the calculation in situ accuracy requirements [20]. The convergence criteria for each time step has been set with an absolute tolerance of 10^{-11}, the normalized concentration lying between 0 and 1. The axisymmetric computational domain is presented in Fig. 1. The bubble is located at the center of a domain of radius R_∞. On the external boundary, inlet and outlet conditions have been imposed. On the left of the domain, the inlet condition consists in imposing a uniform velocity

$$u_L = -U_b \tag{12}$$

Outlet boundary conditions are imposed at the right of the flow domain (Fig. 1): the viscous stress is imposed to zero and a zero pressure reference is chosen

$$\tau_L.\mathbf{n} = 0, \quad p_L = 0 \tag{13}$$

where $\mathbf{n}$ is here the unit vector normal to the external boundary. The boundary conditions imposed at the bubble surface are given by (6). The concentration is set fixed to $c = c_s$ ($c' = 1$) at the bubble surface and the initial concentration is imposed to $c = c_0$ ($c' = 0$) inside the bubble.

We first solve the Navier–Stokes equations (Eqs. (4)–(6)) to obtain the steady velocity field outside and inside the bubble for a given Reynolds number. Then, the transient diffusion–convection equation (Eq. (7)) is solved inside the bubble for different Schmidt numbers in order to vary the Péclet number.

An example of the grid is shown in Fig. 2. Outside the bubble a polar mesh is used, whereas the mesh is triangular inside the bubble. The grid is highly refined in the area near the interface in order to capture the concentration boundary layers. The grid spacing at the interface (both inside and outside) has been determined in order to be much smaller than the concentration boundary layer thickness δ_D estimated by $\delta_D \sim Pe^{-1/2} d_b$. For the maximum Péclet number considered in this study ($Pe = 2000$), the concentration boundary layer thickness δ_D is about $2 \times 10^{-2} d_b$. Four different
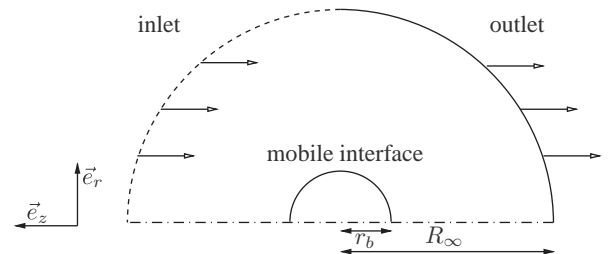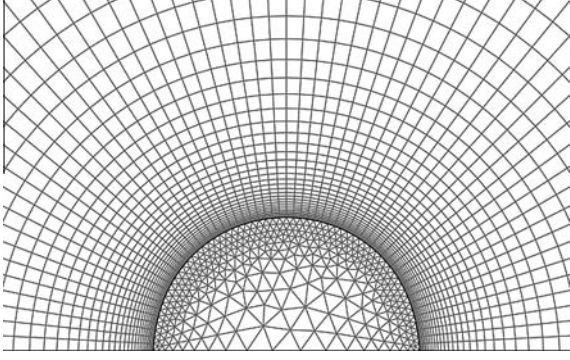

Fig. 1. Computational domain.

Fig. 2. Zoom around the bubble for the mesh A.

Table 1
Internal and external mesh characteristics. N_{in} and N_{out} are the number of cells inside and outside the bubble, Δ_{int} and Δ_{out} are the inside and outside grid spacing at the bubble surface.

	R_∞/r_b	N_{out}	N_{in}	Δ_{out}/d_b	Δ_{in}/d_b
Mesh A	60	3600	645	3.25×10^{-3}	2.38×10^{-2}
Mesh B	120	5000	1201	4.00×10^{-3}	1.50×10^{-2}
Mesh C	60	5500	1327	3.90×10^{-3}	1.31×10^{-2}
Mesh D	60	6000	1498	3.90×10^{-3}	1.25×10^{-2}

meshes (A, B, C and D) have been considered in order to test the confinement imposed by the external boundary located at $r = R_\infty$ from the bubble center, the number of cells N_{in} and N_{out}, the grid spacing at the interface Δ_{in} and Δ_{out} inside and outside the bubble, respectively. The corresponding mesh characteristics are reported in Table 1.

Table 2 presents the values of asymptotic Sherwood number Sh_∞ obtained with the four meshes A, B, C and D for $Pe = 1, 20, 50, 100, 1000, 2000$ and for $Re = 0.1, 10$ and 100. The results found for the different meshes are very close. The largest difference is found with the less refined mesh (mesh A) while no effect is found when increasing the position of the external boundary (mesh B). All the simulations presented in this paper have been performed with the mesh C with $\Delta_{in}/d_b = 1.31 \times 10^{-2}$ and $\Delta_{out}/d_b = 3.90 \times 10^{-3}$. As shown in Table 2 a more refined mesh (mesh D) does not change the results.

4. Preliminary validation

We first report some preliminary validations for the resolution of both the Navier–Stokes equations and the concentration equation.

4.1. Drag coefficient

The bubble drag coefficient C_D is compared with reference results from the literature. The drag force exerted by the surrounding fluid on the bubble is directly calculated from the integration of the

Fig. 3. Drag coefficient vs. bubble Reynolds number: ○ this work; — relation (14) for a clean spherical bubble [21].

pressure and the viscous stress on the bubble surface. In Fig. 3, the drag coefficient C_D is compared with the empirical drag law [21] for clean spherical bubbles:

$$C_D = \frac{16}{Re} \frac{16 + 3.315Re^{1/2} + 3Re}{16 + 3.315Re^{1/2} + Re} \qquad (14)$$

This correlation, that matches the asymptotic analytical solutions for $Re \to 0$ and $Re \to \infty$, has been found in very good agreement with various direct numerical simulations [21–23]. Fig. 3 clearly shows that our numerical results are in good agreement with relation (14).

4.2. Velocity at the bubble interface

As it will be stressed in the following, the tangential velocity at the bubble surface plays an important role in the transfer inside and outside the bubble. Fig. 4.a reports the tangential velocity u_θ versus the polar angle θ for different bubble Reynolds numbers. The velocity distribution is symmetric in the limit of small and large Reynolds number as predicted by the Hadamard–Rybczynski solution and the potential flow, the corresponding maximum velocity located at $\theta = \pi/2$ being $U_{max} = U_b/2$ and $U_{max} = 3U_b/2$, respectively. Fig. 4.b reports the normalized maximal velocity at the interface U_{max}/U_b as a function of the bubble Reynolds number Re. The evolution is compared to the following relation [24]

$$U_{max} = \frac{1}{2} \frac{16 + 3.315Re^{1/2} + 3Re}{16 + 3.315Re^{1/2} + Re} U_b \qquad (15)$$

Both, the local distribution and the maximum value of the tangential velocity at the bubble interface are in very good agreement with previous works [24,25].
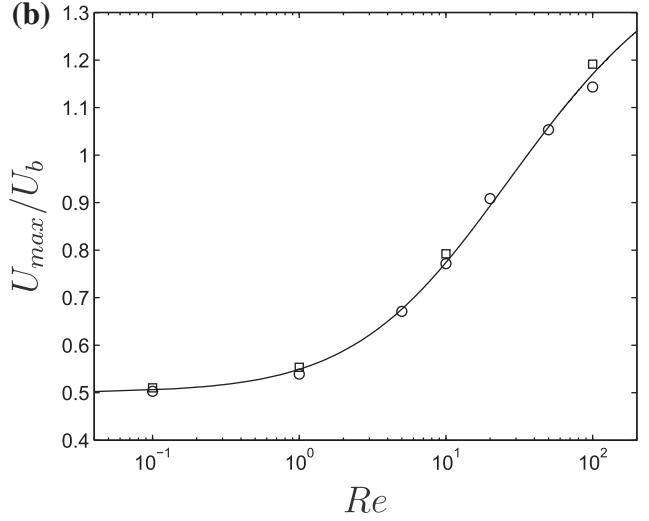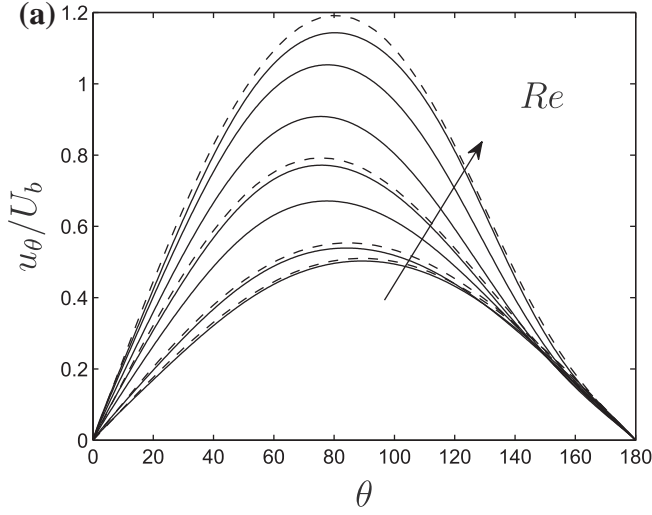
Table 2
Sherwood number Sh_∞ for the meshes A, B, C and D for different Péclet and Reynolds numbers.

Pe	Re = 0.1				Re = 10				Re = 100			
	A	B	C	D	A	B	C	D	A	B	C	D
1	6.56	6.56	6.56	6.56	6.56	6.56	6.56	6.56	6.57	6.57	6.57	6.57
20	7.64	7.63	7.64	7.65	8.66	8.66	8.66	8.66	10.33	10.33	10.31	10.31
50	11.10	11.05	11.09	11.09	13.12	13.11	13.11	13.11	15.01	14.99	14.98	14.99
100	14.58	14.53	14.56	14.57	16.01	15.98	15.99	15.99	16.98	16.95	16.95	16.95
1000	17.68	17.66	17.67	17.67	17.89	17.87	17.87	17.87	17.97	18.02	18.03	18.03
2000	17.73	17.72	17.72	17.72	17.92	17.90	17.90	17.90	17.92	18.04	18.06	18.06

Fig. 4. (a) Velocity at the bubble interface versus the tangential angle θ for different Reynolds number. ($\theta = 0$ is located at the front stagnation point). From bottom to top: $Re = 0.1, 1, 5, 10, 20, 50, 100$. — this study, – – – Legendre et al. [25]. (b) Maximum velocity at the bubble interface vs. bubble Reynolds number: $\circ$ this work, $\square$ Legendre et al. [25], — Eq. (15) Legendre [24].

4.3. Mass transfer in the pure diffusion regime

We first validate the numerical solution of the transfer inside the bubble for the pure diffusion regime ($Re = 0$ and $Pe = 0$). The results are compared to the corresponding analytical solution proposed by Newman [8]. The instantaneous radial profile of the normalized concentration is

$$c'(r', t') = 1 + \frac{2}{r'}\sum_{n=1}^{+\infty}\frac{(-1)^n}{n\pi}exp(-[n\pi]^2 t')sin(n\pi r') \quad \text{for } r' > 0, \quad (16)$$

$$c'(r' = 0, t') = 1 + 2\sum_{n=1}^{+\infty}(-1)^n exp(-[n\pi]^2 t') \quad \text{for } r' = 0, \quad (17)$$

The corresponding instantaneous Sherwood number is given as

$$Sh(t') = \frac{2\pi^2}{3}\frac{\sum_{n=1}^{+\infty}exp(-[n\pi]^2 t')}{\sum_{n=1}^{+\infty}\frac{1}{n^2}exp(-[n\pi]^2 t')} \quad (18)$$

In the limit $t' \to \infty$, Eq. (18) gives the value of the asymptotic Sherwood number $Sh_\infty = 2\pi^2/3 \approx 6.58$ (Eq. (1)). In Fig. 5, some radial profiles are plotted for different dimensionless times. A perfect agreement is obtained between our simulations reported using symbols and the Newman's solution. The corresponding asymptotic Sherwood number estimated from our simulations is $Sh_\infty = 6.56$, which differs only by 0.3% with the Newman's result (1).

4.4. Mass transfer at low Reynolds number

We consider the transfer in the limit of low Reynolds number. We compare our results with available solutions from the literature. The simulations reported in Fig. 6 are performed at $Re = 0.1$. The instantaneous average Sherwood number (Eq. (9)) is plotted against the normalized time t' for different Péclet numbers. As shown in this figure, an interesting agreement is obtained between this work and Clift et al. [4]. The small discrepancy between the

Fig. 5. Instantaneous concentration $c' = (c - c_0)/(c_s - c_0)$ vs. radial position $r' = r/r_b$ for $t' = Dt/r_b^2 = 0.0025, 0.01, 0.025, 0.05, 0.1, 0.15, 0.25, 0.5$: $\circ$ this work for $Re = 0$ and $Pe = 0$. — analytical solution of Newman [8] (Eqs. (16) and (17)).
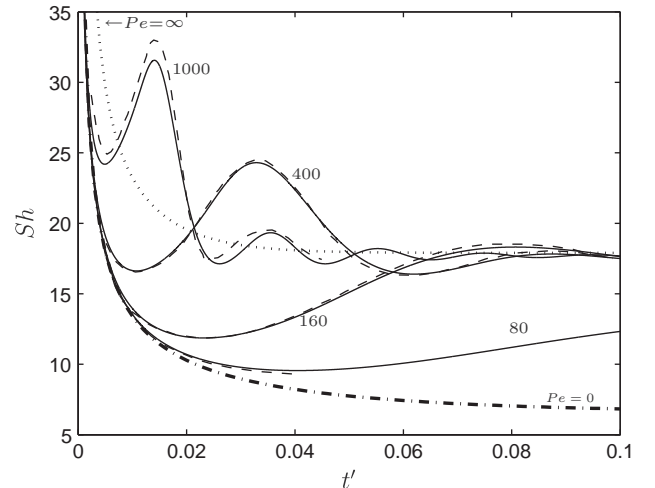
Fig. 6. Instantaneous Sherwood number versus t' for different Péclet numbers at low bubble Reynolds number: – – – Clift et al. [4] for creeping flow; — this work for $Re = 0.1$; – · – analytical solution of Newman [8] for $Pe = 0$ (Eq. (18)); ... relation of Kronig and Brink [11] for $Pe \to \infty$ and $Re \to 0$ (Eq. (19)).

two curves may be explained by the fact that for $Re = 0.1$, the velocity field inside the bubble is not exactly given by the creeping flow solution valid in the limit $Re \rightarrow 0$ [9,10]. A significant difference is observed between our simulations and the Newman's solution (Eq. (18)) due to the value of the Péclet number considered in our simulations. The solution derived by Kronig and Brink [11] is also reported in the figure:

$$Sh(t') = \frac{32}{3} \frac{\sum_{n=1}^{\infty} A_n^2 \lambda_n exp(-16\lambda_n t')}{\sum_{n=1}^{\infty} A_n^2 exp(-16\lambda_n t')} \qquad (19)$$

with the first seven values for A_n and λ_n given by [26]

$$A_n = \begin{bmatrix} 1.33 & 0.60 & 0.36 & 0.35 & 0.28 & 0.22 & 0.16 \end{bmatrix} \qquad (20)$$
$$\lambda_n = \begin{bmatrix} 1.678 & 8.48 & 21.10 & 38.5 & 63.0 & 89.8 & 123.8 \end{bmatrix} \qquad (21)$$

The asymptotic behavior of our simulations (and those of Clift et al. [4]) is correctly reproduced by this solution for $Pe \geqslant 160$. Indeed, our simulations tend with a very good agreement to the corresponding value of the Sherwood number given by relation (2): $Sh_\infty(Re \rightarrow 0, Pe \rightarrow \infty) = 32\lambda_1/3 \approx 17.90$. However, the solution obtained by [11] does not reproduce the time oscillations of the inside transfer observed for the values of the Péclet number considered. These time oscillations, characteristic of the mass transfer inside a fluid sphere [27,4,13,14] results from the inside Hill's vortex [28] whose intensity is controlled by the continuity of the velocity and the viscous shear stress at the interface. This inside convection mechanism is enhanced when increasing the Péclet number. It generates a periodic renewal of the concentration at the interface with fresh fluid particles coming from the bubble axis. Consequently, for a given Reynolds number ($Re = 0.1$ in Fig. 6), the increase of the Péclet number results in time oscillations of the Sherwood number. Due to the enhancement of the inside convection, the asymptotic Sherwood number Sh_∞ increases with the Péclet number as shown in Fig. 6.

5. Results and discussion

We present in Sections 5.1 and 5.2 the results concerning the asymptotic Sherwood number and the saturation time, respectively. Useful simple correlations for the description of the internal mass (or heat) transfer are proposed by introducing a relevant Péclet number based on the maximum tangential velocity U_{max}. Finally, we show in Section 5.3 that this Péclet number is also pertinent for the description of the external mass transfer.

5.1. Sherwood number

The asymptotic Sherwood number Sh_∞ is reported in Fig. 7 versus the Péclet number for $Re = 0.1, 10, 100$. In this figure, the evolution of Sh_∞ with Pe is shown to increase from Newman's solution $Sh_\infty(Pe \rightarrow 0) = 6.58$ up to a finite value close to the Kroning and Brink's result $Sh_\infty(Pe \rightarrow \infty) \approx 17.7 - 18.1$. Therefore, the asymptotic Sherwood number is bounded. This result completely differs from the external transfer where the Sherwood number grows as $Pe^{1/2}$. Moreover, as observed for the external mass transfer [29,5], the increase of the Reynolds number for a given Péclet number, improves the mass transfer resulting in higher values for Sh_∞. Our numerical results are in very good agreement with Clift et al. [4] for $Re = 0.1$ and with the simulations of Juncu [14] (filled symbols) reported for the creeping flow, $Re = 10$ and $Re = 100$. Fig. 7 clearly indicates two asymptotic limits at low and large Péclet number reached for $Pe \leqslant 3$ and $Pe \geqslant 1000$, respectively. It is thus possible to deduce from the figure the corresponding asymptotic Sherwood numbers $Sh_\infty(Re, Pe \rightarrow 0)$ and $Sh_\infty(Re, Pe \rightarrow \infty)$. They are plotted versus the bubble Reynolds number in Fig. 8(a) and (b), respectively. At low Péclet number, $Sh_\infty(Re, Pe \rightarrow 0)$ is found to be
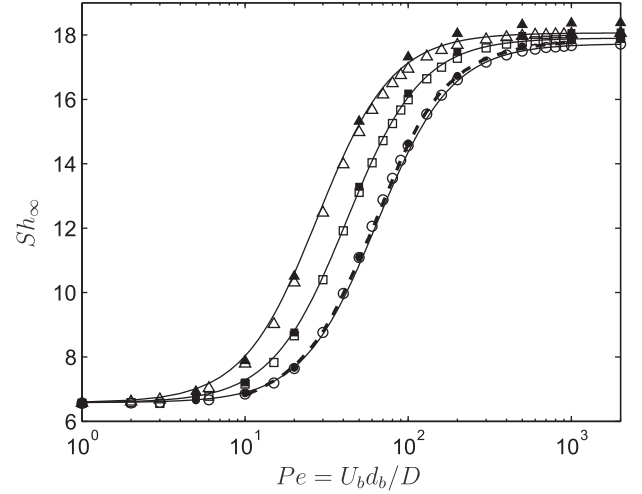

Fig. 7. Sherwood number Sh_∞ vs. Péclet number: – – Clift et al. [4] for creeping flow. This work for $Re = 0.1$ ($\circ$), 10 ($\square$), 100 ($\triangle$). Juncu [14] creeping flow ($\bullet$), $Re=10$ ($\blacksquare$), 100 ($\blacktriangle$); – Eq. (25).

independent on the Reynolds number and $Sh(Re, Pe \rightarrow 0) \approx 6.58$. This value is in very good agreement with the analytical solution (1) of Newman [8] and with the numerical simulations of Juncu [14], the difference being less than 0.15%. The numerical value $Sh_\infty(Re = 0.1, Pe \rightarrow \infty) \approx 17.71$ is also in very good agreement with the solution (2) obtained by Kronig and Brink [11], the difference being around 1%. Fig. 8(b) reports the evolution of $Sh_\infty(Re, Pe \rightarrow \infty)$ normalized by $Sh_\infty(Re \rightarrow 0, Pe \rightarrow \infty)$. $Sh_\infty(Re, Pe \rightarrow \infty)$ slightly increases with the Reynolds number for $Re > 1$. The variation is about $2 - 3\%$ between $Re = 1$ and $Re = 100$ and can be described using the following simple relation:

$$Sh_\infty(Re, Pe \rightarrow \infty) \approx Sh_\infty(Re \rightarrow 0, Pe \rightarrow \infty)(1 + Re)^{0.0044} \qquad (22)$$

The numerical results obtained by Juncu [14] for $Pe = 10^4$ are shown in Fig. 8b. The agreement is very good and reveals the same linear increase with the Reynolds number.

Following Oliver and De Witt [13], Fig. 9 presents the evolution of Sh_∞ against the effective Péclet number Pe_{eff} given by relation (3) for different Reynolds numbers. The numerical results are found to roughly collapse on the evolution obtained by Clift et al. [4] under creeping flow condition. However the observed deviation can be explained by the increase of the transfer with the Reynolds number for a fixed Péclet number. The effective Péclet number Pe_{eff} as expressed by Oliver and De Witt [13] does not seem to be adapted for Reynolds number larger than unity. This point will be discussed in the last section.

In order to improve the modeling of the Sherwood number we introduce the normalized asymptotic Sherwood number Sh_∞^*

$$Sh_\infty^* = \frac{Sh_\infty(Re, Pe) - Sh_\infty(Re, Pe \rightarrow 0)}{Sh_\infty(Re, Pe \rightarrow \infty) - Sh_\infty(Re, Pe \rightarrow 0)} \qquad (23)$$

with $Sh_\infty(Re, Pe \rightarrow 0)$ and $Sh_\infty(Re, Pe \rightarrow \infty)$ given by (1) and (22), respectively. According to Oliver and De Witt [13], the definition of an effective Péclet number was motivated by the following observation: "As the Reynolds number increases, the scaled velocities in the droplet (or bubble) also increase. This increase in velocity is not spatially uniform, thus it is not clear how to account for this increasing velocity with increasing Reynolds numbers". Indeed, as reported in Fig. 4a and b, the interfacial velocity distribution and especially the maximal velocity U_{max} at the interface are strongly affected by the bubble Reynolds number. Consequently, when Re increases, the advection of the concentration at the bubble interface is enhanced. The effective characteristic time scale of the concentra-
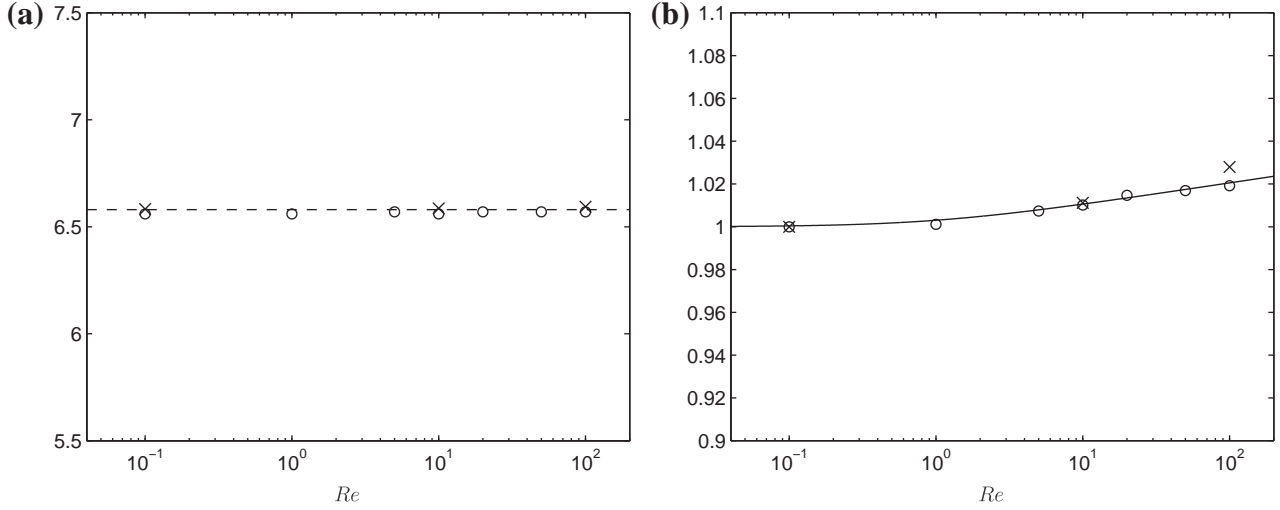
Fig. 8. (a) Sherwood number $Sh_\infty(Re, Pe \to 0)$ versus Re. (b) Sherwood number $Sh_\infty(Re, Pe \to \infty)/Sh_\infty(Re \to 0, Pe \to \infty)$ versus Re. $\circ$ this work, $\times$ Juncu [14], $- - -$ $Sh_\infty(Re \to 0, Pe \to 0) = 6.58$ Newman [8]; $-$ relation (22).
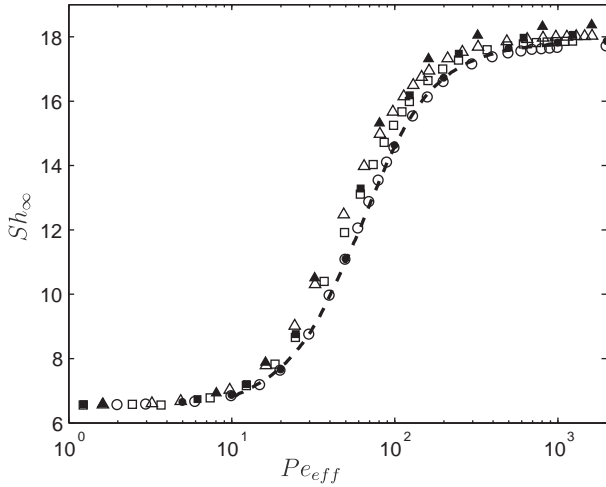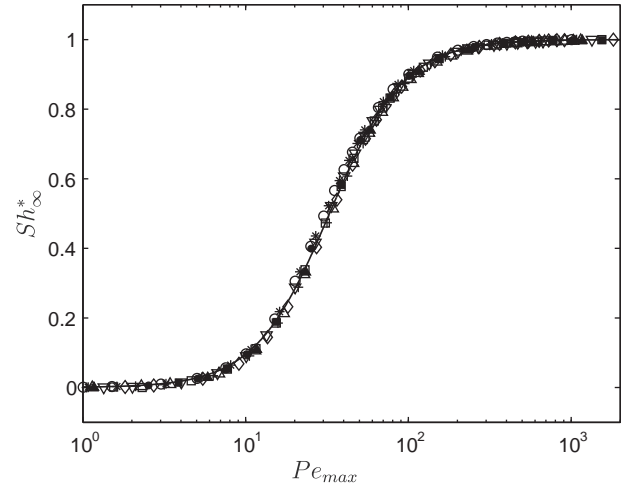

Fig. 9. Sherwood number Sh_∞ vs. the effective Péclet number Pe_{eff} defined by (3). $- - -$ Clift et al. [4] for creeping flow; this work for $Re = 0.1$ ($\circ$), 10 ($\square$), 100 ($\triangle$); Juncu [14]: creeping flow ($\bullet$), $Re=10$ ($\blacksquare$), 100 ($\blacktriangle$).

Fig. 10. Normalized Sherwood number Sh_∞^* vs. Pe_{max}. This work for $Re = 0.1$ ($\circ$), 1 ($*$), 5 ($\triangledown$), 10 ($\square$), 20 ($\diamond$), 50 ($+$), 100 ($\triangle$). Juncu [14]: creeping flow ($\bullet$), $Re=10$ ($\blacksquare$), 100 ($\blacktriangle$). $-$ relation (25) with $\alpha_1 = 1.90$ and $\beta_1 = 3.49$.

tion transport by advection is then $\tau_{adv} = d_b/U_{max}$ that leads to the definition of the Péclet number Pe_{max} defined using the maximal velocity U_{max} at the bubble surface

$$Pe_{max} = \frac{U_{max}d_b}{D} = \frac{U_{max}}{U_b}Pe \qquad (24)$$

Fig. 10 reports the evolution of Sh_∞^* as a function of Pe_{max}. A perfect collapse of all the results is now observed for all the Reynolds number considered ($Re = 0.1, 1, 5, 10, 20, 50, 100$). For a given Péclet number, the enhancement of Sh_∞ with an increase of Re is directly linked to the increase of the maximal velocity U_{max} at the bubble interface. Noting that the Sh_∞^* evolution exhibits a "S" shape, we propose to fit the numerical results by a sigmoid function, as follows

$$Sh_\infty^* = \frac{1}{1 + \exp\left(-\alpha_1[\ln(Pe_{max}) - \beta_1]\right)} \qquad (25)$$

The least squares method is used to estimate α_1 and β_1. As shown in Figs. 7 and 10, Eq. (25) with $\alpha_1 = 1.89$ and $\beta_1 = 3.49$ describes the

evolution of Sh_∞^*. The results of Juncu [14] (filled symbols) are also in perfect agreement.

5.2. Saturation time

The time t_{sat} necessary to achieve the saturation of the bubble is now considered. This parameter is of importance for the complete modeling of the mass (or heat) transfer. We define here the saturation time t_{sat} as the time to reach 99% of the final concentration inside the bubble, i.e. $F = 0.99$. t_{sat} is reported in Fig. 11 versus the Péclet number for $Re = 0.1, 10, 100$. For a given Péclet number, the improvement of mass transfer by increasing the Reynolds number generates a lower saturation time. This behavior is clearly related to the increase of the Sherwood number with the bubble Reynolds number. t_{sat} is found to decrease from the value deduced from the analytical solution (16) and (17)

$$t_{sat}(Re, Pe \to 0) = 0.416 \frac{r_b^2}{D} \qquad (26)$$

The numerical value $t_{sat}(Re = 0.1, Pe \to \infty) = 0.158 r_b^2/D$ is in very good agreement with the value $t_{sat}(Re \to 0, Pe \to \infty) = 0.155 r_b^2/D$
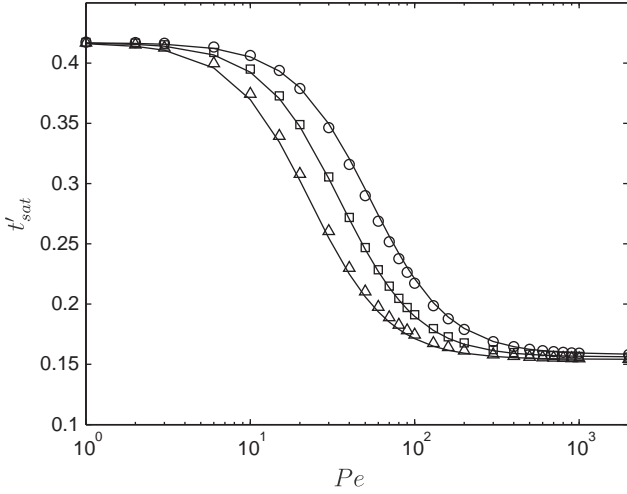
Fig. 11. Saturation time $t'_{sat} = t_{sat}D/r_b^2$ vs. Péclet number. This work for Re = 0.1 (○), 10 (□), 100 (△). — relation (29)

obtained from the solution derived by Kronig and Brink [11]. $t_{sat}(Re, Pe \rightarrow \infty)$ is found to vary in the range $0.154 - 0.158\, r_b^2/D$ for the Reynolds numbers considered. This evolution can be described using the following relation valid for $Re \leqslant 100$

$$t_{sat}(Re, Pe \rightarrow \infty) = t_{sat}(Re \rightarrow 0, Pe \rightarrow \infty)(1 + Re)^{-0.0054} \quad (27)$$

We now define the normalized saturation time t^*_{sat} as

$$t^*_{sat} = \frac{t_{sat}(Re, Pe) - t_{sat}(Re, Pe \rightarrow \infty)}{t_{sat}(Re, Pe \rightarrow 0) - t_{sat}(Re, Pe \rightarrow \infty)} \quad (28)$$

where $t_{sat}(Re, Pe \rightarrow 0)$ and $t_{sat}(Re, Pe \rightarrow \infty)$ are given by (26) and (27), respectively. Fig. 12 reports the evolution of t^*_{sat} as a function of Pe_{max}. As shown by the figure, all the evolutions collapse on the same curve. The following relation based on a sigmoid function describes the corresponding evolution:

$$t^*_{sat} = 1 - \frac{1}{1 + \exp\left(-\alpha_2 [\ln(Pe_{max}) - \beta_2]\right)} \quad (29)$$

with $\alpha_2 \approx 1.81$ and $\beta_2 \approx 3.30$. Fig. 11 confirms that relation (29) gives a good description of the saturation time for all the values (Re, Pe) considered in this study.
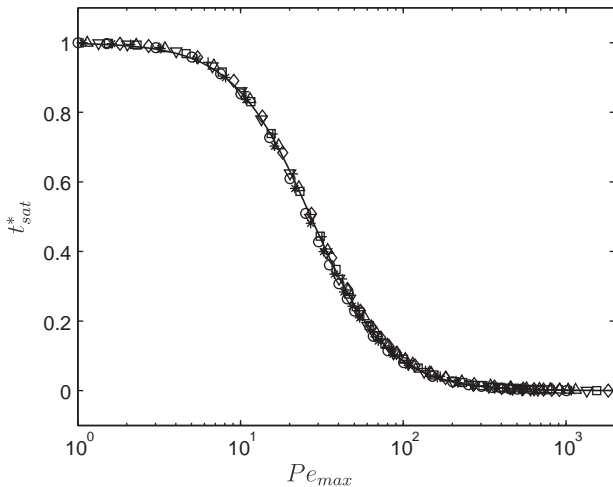
Fig. 12. Normalized saturation time t^*_{sat} vs. Pe_{max}. This work for Re = 0.1 (○), 1 (∗), 5 (▽), 10 (□), 20 (◇), 50 (+), 100 (△). — relation (29) with $\alpha_2 = 1.81$ and $\beta_2 = 3.30$.

5.3. External mass (or heat) transfer

We finally extend the previous analysis to the external mass transfer. As shown in Figueroa and Legendre [7], the correlations of Winnikow [29] and Takemura and Yabe [5] are very useful to describe the external Sherwood number Sh^{ext}_∞. These two relations are able to predict the increase of the Sherwood number induced by an increase of the Reynolds number. However, the relation derived by Winnikow [29], based on the tangential velocity derived by Moore [30], is only valid for $Re > 50$. Moreover, the relation of Takemura and Yabe [5] is also not able to reproduce the pure diffusion limit $Sh^{ext}_\infty = 2$, when both the Reynolds and the Péclet numbers tend to zero. Consequently, there is not a general relation equivalent to relation (25) available for the description of the external transfer whatever the Reynolds and Péclet numbers considered.

For the discussion reported in this section, no additional simulation for the external transfer has been performed because of the large amount of results available in the literature. The external Sherwood number Sh^{ext}_∞ values have been collected from several numerical studies [31–33,7]. Fig. 13 reports Sh^{ext}_∞ as a function of the external Péclet number $Pe^{ext} = U_b d_b / D_L$ where D_L is the diffusion coefficient in the liquid surrounding the bubble. The plot clearly outlines the effect of the Reynolds number on the transfer for a given Péclet number. The numerical values of Sh^{ext}_∞ are compared in Fig. 13 with several relations from the literature. Based on available numerical data, Clift et al. [4] proposed the following correlation valid under creeping flow conditions:

$$Sh^{ext}_\infty(Re \rightarrow 0, Pe^{ext}) = 1 + \left[1 + 0.564\,(Pe^{ext})^{2/3}\right]^{3/4} \quad (30)$$

As shown in Fig. 13, the results of Saboni et al. [33] for creeping flow (+) and the results of Legendre and Magnaudet [31] for low Péclet number at $Sc = 1$ (●) are in good agreement with relation (30). Note that, relation (30) is consistent with both the analytical asymptotic solution in the limit of low Péclet number [34]

$$Sh^{ext}_\infty(Re \rightarrow 0, Pe^{ext} \rightarrow 0) = 2 + \frac{1}{2} Pe^{ext} \quad (31)$$

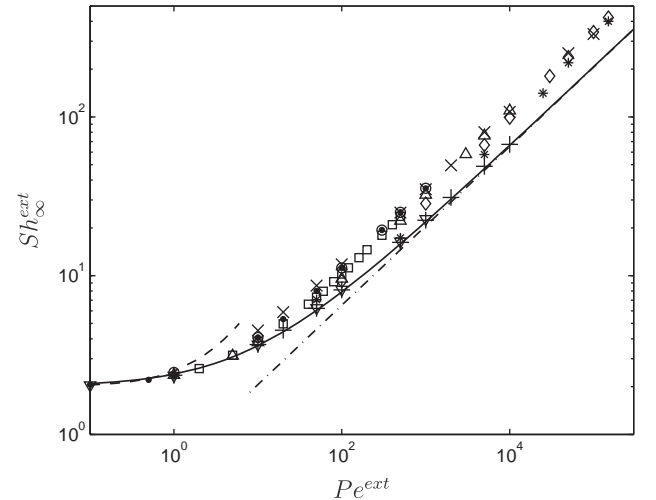and the solution obtained in the limit of high Péclet number [35]:

Fig. 13. Asymptotic Sherwood number Sh^{ext}_∞ for external mass transfer versus the external Péclet number Pe^{ext}. Numerical simulations of Legendre and Magnaudet [31] for ● $Sc = 1$ varying Re; Numerical simulations of Dani et al. [32] for ▽ Re = 0.01 varying Sc, □ Sc = 2 varying Re; Numerical simulations of Saboni et al. [33] for + creeping flow and for × Re = 400 varying Sc; Numerical simulations of Juncu [7] for o Sc = 1, △ Sc = 10, ◇ Sc = 100, ∗ Sc = 500 varying Re; — Eq. (30) [4], – – – Eq. (31) Brenner [34], – · – Eq. (32) Lochiel and Calderbank [35].

$$Sh_\infty^{ext}(Re \to 0, Pe^{ext} \to \infty) = \frac{2}{\sqrt{3}\,\pi}\left(Pe^{ext}\right)^{1/2} \tag{32}$$

The objective is now to consider the Péclet number $Pe_{max}^{ext} = U_{max}d_b/D_L$ based on the maximum tangential velocity U_{max} for the description of the external mass (or heat) transfer. The external Sherwood number Sh_∞^{ext} is reported as a function of Pe_{max}^{ext} in Fig. 14. As shown for the internal transfer, all the numerical results are found to collapse on a single curve. The Péclet number Pe_{max}^{ext} based on the maximal velocity at the bubble surface is also the pertinent parameter for the description of the external transfer. Fig. 14 also reveals that the following relation based on relation (30) describes the evolution of Sh_∞^{ext}

$$Sh_\infty^{ext} = 1 + \left[1 + \left(\frac{4}{3\pi}\right)^{2/3}\left(2\,Pe_{max}^{ext}\right)^{2/3}\right]^{3/4} \tag{33}$$

where the approximate value 0.564 in relation (30) has been replaced by the exact one $(4/3\pi)^{2/3}$ deduced from the analytical solution (32). In the limit of both large Reynolds number and large Péclet number $Pe_{max}^{ext} \to 3/2\,Pe^{ext}$, relation (33) tends to the Boussinesq solution [36]:

$$Sh_\infty^{ext}(Re \to \infty, Pe^{ext} \to \infty) \to \frac{2}{\sqrt{\pi}}\left(Pe^{ext}\right)^{1/2} \tag{34}$$

Consequently, relation (33) provides an accurate description of the external mass (or heat) transfer for a complete range of both the bubble Reynolds number and the Péclet number.

5.4. On the effective Péclet number

The results presented above indicate that the relevant parameter for the description of both the internal (resp. external) mass (or heat) transfer is the Péclet number Pe_{max} (resp. Pe_{max}^{ext}) based on the maximum velocity at the bubble surface. Fig. 14 shows that relation (33) deduced from relation (30) describes the evolution of the Sherwood number for all the values (Re, Pe) considered. As a consequence the so-called effective Péclet number [13] is $Pe_{eff} = 2$-Pe_{max}. Thus, the effective Péclet number can be described for all the values of both the Reynolds number and the Péclet number as

$$Pe_{eff} = \frac{16 + 3.315 Re^{1/2} + 3Re}{16 + 3.315 Re^{1/2} + Re}\,Pe \tag{35}$$
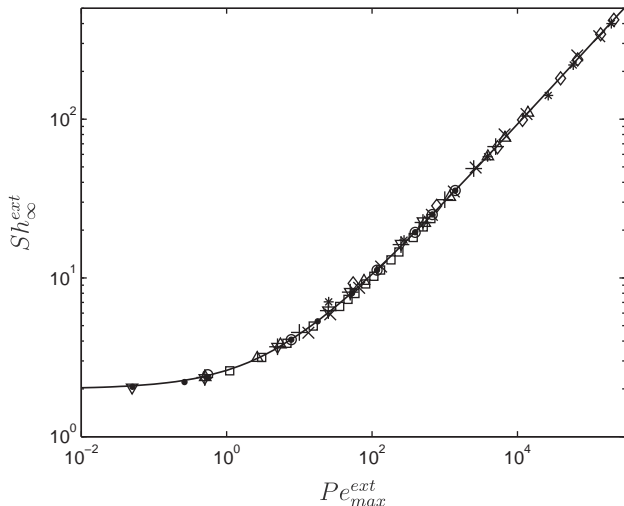

Fig. 14. Sherwood number Sh_∞^{ext} for external mass transfer versus the maximal Péclet number Pe_{max}^{ext}. symbols: same legend as in Fig. 13; − relation (33).
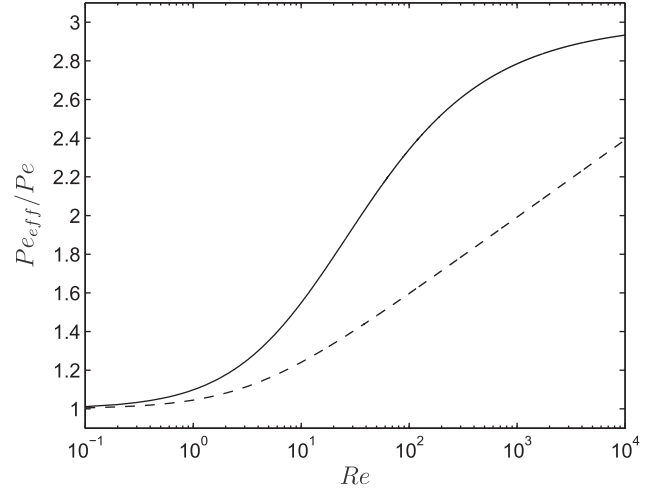

Fig. 15. Effective Péclet number Pe_{eff} as a function of the Reynolds number. − − − relation (3), relation (35).

The evolution of Pe_{eff}/Pe is reported in Fig. 15 as a function of the Reynolds number. Due to the variation of the maximum velocity at the bubble surface with the Reynolds number, the value of the effective Péclet number is tripled between the limit at low Reynolds number and the limit at high Reynolds number. The effective Péclet number proposed by Oliver and De Witt [13] (relation (3)) is also shown in Fig. 15. The two relations are in agreement at very low Reynolds number. This is consistent with Fig. 9 where the agreement with relation (30) is shown for $Re = 0.1$.

Finally, the results presented in this study indicate that both the internal and external mass (or heat) transfer can be described using the same effective Péclet number given by relation (35).

6. Conclusions

The mass (or heat) transfer inside a spherical clean bubble in a uniform flow has been considered by means of numerical simulation. Simulations were performed for Péclet number up to $Pe = 2000$ for a large range of the bubble Reynolds number $(0.1 \leqslant Re \leqslant 100)$. The effects of both the Reynolds number and the Péclet number have been discussed by considering the evolution of the Sherwood number and the saturation time. For a fixed Péclet number, the transfer is increased when increasing the Reynolds number because the strength of the internal recirculation is enhanced. This study has revealed that the Péclet number Pe_{max} based on the maximum tangential velocity at the bubble surface is the relevant parameter for the description of the transfer. The analysis has been extended to the external mass (or heat) transfer. Considering results from the literature we have shown that Pe_{max} is also the pertinent parameter. Future works could confirm that Pe_{max} is still relevant for the description of the transfer for larger Péclet and Reynolds numbers. It should be also very interesting to extend a similar analysis to partially contaminated bubbles, deformable bubbles and fluid spheres with higher viscosity ratio.

In this study we have considered the transfer inside a clean, spherical bubble with a fixed radius in a uniform steady flow. The objective was to improve the knowledge of the inside transfer since most of the previous studies have considered the external transfer for the same configuration. Such results for the transfer can then be used for the modeling of complex bubbly flows and are more or less valid depending on the case under consideration. Typically, it is supposed to give a good description of the transfer for dilute bubbly flows (less than 1or 2 percent) and if the flow seen by the bubble is uniform at the bubble scale (i.e. if the bubbles

are much smaller than the smallest scale of the flow). In addition, the results are obtained considering a fixed radius. Such quasi-steady evolution is in practice reasonable if the characteristic time scales of the transfer (diffusion and advection) are much smaller than the characteristic time of the radius evolution. However, the recent experiments of [37] have shown that the corresponding deduced models for the external transfer can be used for a good prediction of the transfer in a dense bubble swarm up to void fraction of about 16.5%. Such experimental results make us confident that the results obtained under academic configuration are very useful for the modeling of complex bubbly flows.

Acknowledgments

References

[1] W. Lewis, G. Whitman, Principles of gas absorption, Ind. Eng. Chem. 16 (1924) 1215–1220.
[2] D.W. Green and R.H. Perry, Perry's chemical engineers' handbook, 2007, McGraw-Hill, 8th Edition
[3] M. Roustan, Transfert Gaz-Liquide dans les procédés de traitement des eaux et des effluents gazeux, Tec & Doc, Lavoisier, Paris, 2003.
[4] R. Clift, J. Grace, M. Weber, Bubles Drops and Particules, Academic Press, San Diego, 1978.
[5] F. Takemura, A. Yabe, Gas dissolution process of spherical rising bubbles, Chem. Eng. Sci. 53 (1998) 2691–2699.
[6] E. Michaelides, Particles Bubbles and Drops: Their Motion, Heat and Mass Transfer, World Scientific Pub. Co. Inc., 2006.
[7] B. Figueroa, D. Legendre, Mass or heat transfer from spheroidal gas bubbles rising through a stationary liquid, Chem. Eng. Sci. 65 (2010) 6296–6309.
[8] A. Newman, The drying of porous solid diffusion and surface emission effects, Trans. Am. Inst. Chem. Eng. 27 (1931) 203–220.
[9] J. Hadamard, Mouvement permanent lent d'une sphère liquide et visqueuse dans un liquide visqueux, C.R. Acad. Sci. Paris 152 (1911) 1735–1738.
[10] W. Rybczynski, Uber die fortschreitende Bewegung einer flussigen Kugel in einem zahen Medium, Bull. Acad. Sci. Cracovie Ser. A, Poland (40).
[11] R. Kronig, J. Brink, On the theory of extraction from falling droplets, Appl. Sci. Res. A2 (1950) 142–154.
[12] P. Calderbank, I. Korchinski, Circulation in liquid drops: (a heat-transfer study), Chem. Eng. Sci. 6 (1956) 65–78.
[13] D. Oliver, K. De Witt, Heat transfer in bubbles and droplets at moderate Reynolds numbers: interior problem, Am. Inst. Chem. Eng. Symp. Ser. 306 (91) (1995) 87–92.
[14] G. Juncu, A numerical study of the unsteady heat/mass transfer inside a circulating sphere, Int. J. Heat Mass Transfer 53 (2010) 3006–3012.
[15] A. Paschedag, W. Piarah, M. Kraume, Sensitivity study for the mass transfer at a single droplet, Int. J. Heat Mass Transfer 48 (16) (2005) 3402–3410.
[16] N. Zaritzky, A. Calvelo, Internal mass transfer coefficient within single bubbles. Theory and experiment, Can. J. Chem. Eng. 57 (1) (1979) 58–64.
[17] L. Milne-Thomson, Theoretical Hydrodynamics, McMillan, New York, 1960.
[18] A. Blanco, J. Magnaudet, The structure of the axisymmetric high-Reynolds number flow around an ellipsoidal bubble of fixed shape, Phys. Fluids 7 (6) (1995) 1265–1274.
[19] O. Schenk, K. Gärtner, Solving unsymmetric sparse systems of linear equations with pardiso, J. Future Gener. Comput. Syst. 20 (3) (2004) 475–487.
[20] A. Hindmarsh, P. Brown, K. Grant, S. Lee, R. Serban, D. Shumaker, C. Woodward, Sundials: suite of nonlinear and differential/algebraic equation solvers, ACM Trans. Math. Software 31 (2005) 363.
[21] R. Mei, J. Klausner, C. Lawrence, A note on the history force on a spherical bubble at finite reynolds number, Phys. Fluids 6 (1994) 418.
[22] S. Takagi, Y. Matsumoto, Force acting on a rising bubble in a quiescent fluid., Proc. ASME Summer Meeting Numer. Methods Multiphase Flow San Diego (1996) 575–580.
[23] D. Legendre, J. Magnaudet, Force acting on a rising bubble in a quiescent fluid., J. Fluid Mech. 368 (1998) 81–126.
[24] D. Legendre, On the relation between the drag and the vorticity produced on a clean bubble, Phys. Fluids 19 (2007) 018102.
[25] D. Legendre, V. Sarrot, P. Guiraud, On the particle inertia-free collision with a partially contaminated spherical bubble, Int. J. Multiphase Flow 35 (2009) 163–170.
[26] P. Heertjes, W. Holve, H. Talsma, Mass transfer between isobutanol and water in a spray-column, Chem. Eng. Sci. 3 (3) (1954) 122–142.
[27] H. Watada, A. Hamielec, A. Johnson, A theoretical study of mass transfer with chemical reaction in drops, Can. J. Chem. Eng. 48 (3) (1970) 255–261.
[28] M. Hill, On a spherical vortex, Philos. Trans. R. Soc. A 185 (1894) 213–245.
[29] S. Winnikow, Letters to the editor, Chem. Eng. Sci. 22 (1967) 22–477.
[30] D. Moore, The boundary layer on a spherical gas bubble, J. Fluid Mech. 16 (1963) 161–176.
[31] D. Legendre, J. Magnaudet, Effet de l'accélération d'un écoulement sur le transfert de masse ou de chaleur à la surface d'une bulle sphérique, C.R. Acad. Sci. Paris Sér. IIb, France 327 (1999) 63–70.
[32] A. Dani, A. Cockx, P. Guiraud, Direct numerical simulation of mass transfer from spherical bubbles: the effect of interface contamination at low Reynolds numbers, Int. J. Chem. Reactor Eng. 4 (1) (2006).
[33] A. Saboni, A. Alexandrova, A. Spasic, C. Gourdon, Effect of the viscosity ratio on mass transfer from a fluid sphere at low to very high Péclet numbers, Chem. Eng. Sci. 62 (2007) 4742–4750.
[34] H. Brenner, Forced convection heat and mass transfer at small Péclet numbers from a particle of arbitrary shape, Chem. Eng. Sci. 18 (1963) 109–122.
[35] A. Lochiel, P. Calderbank, Mass transfer in the continuous phase around axisymmetric bodies of revolution, Chem. Eng. Sci. 19 (1964) 471–484.
[36] J. Boussinesq, Calcul du pouvoir refroidissant des courants fluides, J. Math. Pures Appl. 6 (1905) 285–332.
[37] D. Colombet, D. Legendre, A. Cockx, P. Guiraud, F. Risso, C. Daniel, S. Galinat, Experimental study of mass transfer in a dense bubble swarm, Chem. Eng. Sci. 66 (2011) 3432–3440.